

Numerical Experiment on the Circulation in the Japan Sea

Part II. Influence of Seasonal Variations in Atmospheric Conditions on the Tsushima Current*

Jong-Hwan YOON**

Abstract: Seasonal variations in the circulation in the Japan Sea are investigated numerically by using a model basin of uniform depth with three openings, one inflow opening corresponding to the Tsushima Straits and two outflow openings corresponding to the Tsugaru- and Sôya Straits.

From winter to spring, warm water supplied through the inflow opening flows northward along the Korean coast as a western boundary current corresponding to the East Korean Warm Current. From summer to autumn, the warm water splits into two branches; one flows northward along the Korean coast as from winter to spring and the other flows along the Japanese coast as a density-driven boundary current due to the large density difference between the inflowing warm and low salinity water and the interior water which was cooled during winter.

The lack of a boundary current along the Japanese coast from winter to spring results in a large discrepancy between calculated and observed salinity field distributions. Therefore, the nearshore branch of the Tsushima Current can not be explained only as a density-driven boundary current.

The seasonal variation of atmospheric conditions plays an important role in the formation of the Proper Water and the Polar Front in the Japan Sea.

1. Introduction

According to the results of numerical experiment by YOON (1982), the warm water supplied through a southern opening in a rectangular ocean, does not split into two branches under annual mean atmospheric conditions, and only a western boundary current exists, corresponding to the East Korean Warm Current.

In this paper, it is investigated numerically whether seasonal variations in atmospheric conditions are important in the splitting of the Tsushima Current and in forming the Polar Front in the Japan Sea.

The numerical model is designed so as to represent oceanic and atmospheric conditions as realistically as possible with the exception of the bottom topography (a flat bottom is assumed in this model).

2. Model

A schematic view of the model ocean is shown in Fig. 1. The ocean basin with a uniform depth of 1,500 m has three straits (the Tsushima-, the Tsugaru- and the Sôya Straits) whose depths are 150 m. The width of the Tsushima Strait is 198 km and those of the Tsugaru- and the Sôya Straits are 66 km. A rectangular coordinate system on a β -plane is used, taking x

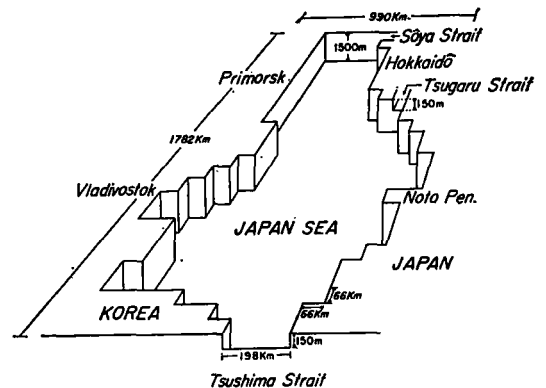


Fig. 1. Schematic view of the model ocean.

* Received Aug. 7, 1981, revised Mar. 9 and accepted Apr. 12, 1982.

** Geophysical Institute, Faculty of Science University of Tokyo, Bunkyo-ku, Tokyo 113, Japan

south-eastward, y north-eastward, and z upward from the mean sea surface level. Let u , v and w be components of velocity in the x , y and z direction, respectively. The equations of motion (the Navier-Stokes equation) are simplified by making the Boussinesq and hydrostatic approximations.

The Coriolis parameter in this coordinate system is $f=f_0+\beta(x \sin 45^\circ+y \sin 45^\circ)$, where β is the latitudinal variation of f . In this study, the effect of salinity on density is taken into account. The conservation equations of temperature T and salinity S and the equation of state are

$$T_t + \mathcal{L}T = K_v T_{zz} + K_h (T_{xx} + T_{yy}), \quad (1)$$

$$S_t + \mathcal{L}S = K_v S_{zz} + K_h (S_{xx} + S_{yy}), \quad (2)$$

$$\rho = F(T, S, p), \quad (3)$$

where K_v and K_h are coefficients of the vertical and horizontal eddy diffusion, respectively. The convective adjustment mechanism is introduced in the model to maintain the stable stratification. The advection operator \mathcal{L} is defined by

$$\mathcal{L}\mu = (u\mu)_x + (v\mu)_y + (w\mu)_z \quad (4)$$

The functional form of $F(T, S, p)$ is approximated by a polynomial, whose coefficients are fitted to the standard Knudsen formula. Details are given in FRIEDRICH and LEVITUS (1972). At vertical walls each of the velocity components and the heat and salt flux are zero. At the ocean floor, the momentum, heat and salt flux are zero. Motion is forced at the southern opening by imposing the mass, thermal and salt flux, and at the ocean surface by imposing the thermal flux and wind stress. The salt flux due to evaporation and precipitation at the ocean surface is not considered.

To obtain fields of wind stress, mean geostrophic wind velocities \mathbf{V}_g at the ocean surface are calculated from maps of monthly mean atmospheric pressure (JAPAN METEOROLOGICAL AGENCY, 1971: pls. 53-58). Stresses due to the wind are computed by using a drag law

$$|\boldsymbol{\tau}| = |(\tau^x, \tau^y)| = \rho_A \times 1.4 \times 10^{-3} |\mathbf{V}_g|^2 \quad (5)$$

where $\rho_A (=1.2 \times 10^{-3} \text{ g cm}^{-3})$ is the density of air, and assuming a turning angle of 20° in the atmospheric boundary layer.

The boundary conditions for temperature at the surface are specified in Section 4 and the boundary conditions in the straits for temperature, salinity and velocity are specified in Section 3.

The following values are used for the numerical experiment: $f_0 = 2\Omega \sin 39^\circ = 0.9153 \times 10^{-4} \text{ s}^{-1}$, $\beta = 1.8 \times 10^{-13} \text{ cm}^{-1} \text{ s}^{-1}$, A_h (horizontal eddy viscosity) $= 1.5 \times 10^7 \text{ cm}^2 \text{ s}^{-1}$, $K_h = 1.0 \times 10^6 \text{ cm}^2 \text{ s}^{-1}$, $A_v = K_v = 0.5 \text{ cm}^2 \text{ s}^{-1}$, where Ω is the rate of rotation of the earth. The horizontal grid interval is 66 km. Since the Munk's width of the western boundary layer $\frac{2\pi}{\sqrt{3}} (A_h/\beta)^{1/3}$ is 158 km for the above parameters, this grid interval is less than the width of the viscous western boundary layer. In the vertical direction, we take eight layers as shown in Table 1. The time interval (Δt) in numerical calculations is taken to be two hours.

The numerical method in the present study is basically the same as that described by BRYAN (1969).

3. Conditions at the openings

MIYAZAKI (1952) and YI (1966) studied the seasonal variation of volume transport through the Tsushima Straits on the basis of geostrophic calculations referred to the bottom. MIYAZAKI (1952) concluded that the transport had a large seasonal variation and had a maximum value ($2.5 \times 10^{12} \text{ cm}^3 \text{ s}^{-1}$) in summer and a minimum value ($0.2 \times 10^{12} \text{ cm}^3 \text{ s}^{-1}$) in winter. YI (1966) obtained almost the same results as those of MIYAZAKI. But it seems that they underestimated the transport because the Tsushima Strait is very shallow and the velocities near the bottom might have significant values (MIITA, 1976) at all seasons, and they overestimated the relative difference of transport between winter and summer because the vertical homogeneity

Table 1. Thickness of each layer.

Layer	1st	2nd	3rd	4th	5th	6th	7th	8th
Thickness	30m	30m	40m	50m	80m	160m	320m	790m

Table 2. Vertical distribution of velocity normal to the transverse section of the Tsushima Strait.

Layer	Thickness (m)	Normal velocity (cm s^{-1})
1st	30	15.0
2nd	30	10.0
3rd	40	4.0
4th	50	2.0

of the Tsushima Current in winter would significantly reduce the transport on the basis of geostrophic calculation referred to the bottom.

MIITA (1976) summarized the data on current velocity measured by current-meters in the Tsushima Strait from 1924 to 1974 and concluded that the volume transport through the Tsushima Strait is $3.3 \times 10^{12} \sim 3.7 \times 10^{12} \text{ cm}^3 \text{ s}^{-1}$ in summer. Because of the very limited data in winter, he did not estimate the volume transport in winter.

Because of the insufficiency of information on the seasonal variation in volume transport through the Tsushima Strait, it is taken to be constant ($2.0 \times 10^{12} \text{ cm}^3 \text{ s}^{-1}$) in the present model. The vertical distribution of the velocity normal to a transverse section in the Tsushima Strait is shown in Table 2. These values are assumed not to vary horizontally in the transverse section. Though the seasonal variations of temperature and salinity in the Tsushima Strait are taken into account, the velocity values are fixed throughout the calculation. The slippery condition for the component of velocity tangential to this transverse section is adopted. The imposed seasonal changes in vertical distributions of salinity and reference temperature $T_R(z)$ in the Tsushima Strait are shown in Fig. 2. These distributions are determined on the basis of the monthly mean vertical sections of temperature and salinity in the east channel of the Tsushima Strait reported by NAN'NITI and FUJIKI (1967). Temperature and salinity in winter are vertically uniform. The minimum temperature occurs in February and has a value of 13.5°C , and the maximum salinity occurs in April and has a value of 34.65‰ . In summer, vertical stratification develops. Temperature has a maximum value of 25.5°C in September, and salinity a minimum value of 32.70‰ in August in the surface layer. The distribution of salinity

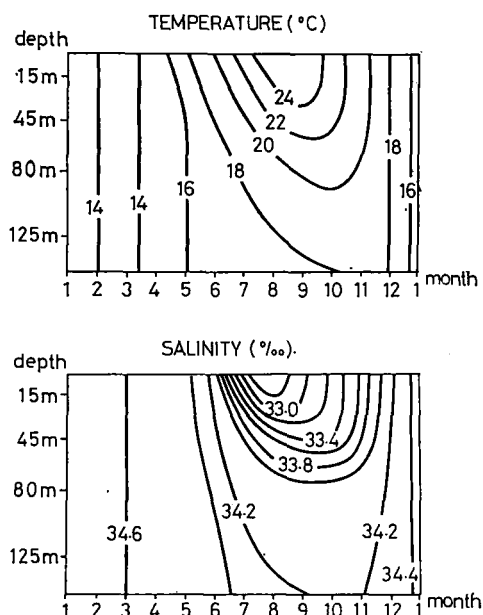


Fig. 2. Imposed seasonal changes of vertical distributions of the reference temperature $T_R(z)$ (upper) and salinity S (lower) at the Tsushima Strait.

along the transverse section in the Tsushima Strait is taken to be uniform in the horizontal direction. The distribution of temperature $T_0(x, z)$ in the transverse section is given by

$$T_0(x, z) = T_R(z) + a(x - b) \quad (6)$$

where x is the distance from the south-west side of the Tsushima Strait and a and b are the constants of $(1/33)^\circ\text{C km}^{-1}$ and 132 km respectively.

The values of outflow volume transport through the Tsugaru Strait (V_2) and the Sōya Strait (V_3) are assumed to be

$$\begin{aligned} V_2 &= 0.65 V_1 \\ V_3 &= 0.35 V_1, \end{aligned} \quad (7)$$

where V_1 denotes the inflow volume transport through the Tsushima Strait.

The boundary conditions at the outflow openings are given by

$$\begin{aligned} u_y = T_y = S_y = 0, \quad v = v_a + F_1 \\ \text{for the Tsugaru Strait,} \end{aligned} \quad (8)$$

and

Table 3. Three experiments carried out in the present study.

Experiment	Drag coefficient	Atmospheric conditions	Period of time integration
I	$(1.0+0.0007V_A)\times 10^{-3}$	Linear interpolations of monthly mean values	4 years
II	$(1.0+0.0007V_A)\times 10^{-3}$	Linear interpolations of monthly mean values +short term fluctuations	7 years
III	$(0.80+0.00114V_A)\times 10^{-3}$	Linear interpolations of monthly mean values +short term fluctuations	9 years

$$v_x = T_x = S_x = 0, \quad u = u_a + F_2$$

for the Sôya Strait, (9)

where u_a and v_a are the x and y components of velocities on the interior grid points adjacent to the outflow openings, respectively. Since the outflow openings have just one grid point, the constant values F_1 and F_2 are determined so as to equate the volume transports through the openings to the values in (7):

$$F_1 = \frac{V_2}{hl} - \frac{1}{h} \int_{-h}^0 v_a dx$$

$$F_2 = \frac{V_3}{hl} - \frac{1}{h} \int_{-h}^0 u_a dx$$

(10)

where h and l are the depth (150 m) and the width (66 km) of the outflow openings.

4. Thermal boundary conditions at the sea surface

The formulation of thermal boundary conditions at the sea surface is similar to that described by HANEY (1971). Details of the formulation are given in Part I (YOON, 1982).

In the present model, the ocean surface temperature T_s is replaced with the temperature T_1 at the first level below the ocean surface by assuming that the sub-surface layer is always well-mixed.

Three experiments are carried out as shown in Table 3, where two different formulae for the drag coefficient C_D are used. One formula which was proposed by DEACON and WEBB (1962),

$$C_D = (1.0 + 0.0007 V_A) \times 10^{-3}, \quad (11)$$

is used in Experiments I and II, and the other which was proposed by SHEPPARD (1958)

$$C_D = (0.8 + 0.00114 V_A) \times 10^{-3}, \quad (12)$$

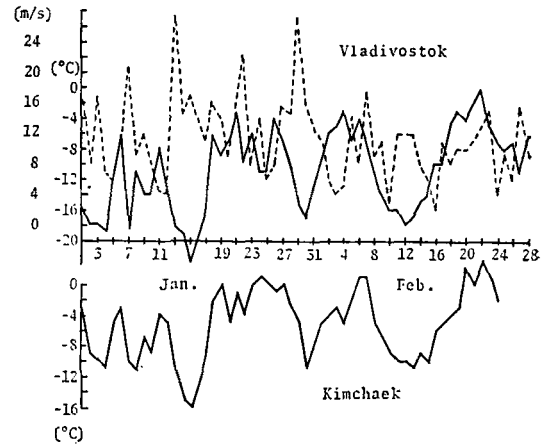


Fig. 3. Meteorological data at Vladivostok and Kimchaek (North Korea) in winter, 1967 (solid line: air temperature, broken line: wind speed) (after FUKUOKA and MISUMI, 1977).

is used in Experiment III.

The instantaneous values of meteorological elements such as air temperature T_A , relative humidity γ , cloud amount n_C and wind speed V_A (cm s^{-1}) used in Experiment I are obtained by linearly interpolating the monthly mean values averaged for 12 years from 1958 to 1969 (MAIZURU MARINE OBSERVATORY, 1972). The monthly mean amount of Q_{s0} (solar radiation in a cloudless atmosphere) is given by BUDYKO (1974: pp 1-11).

The negative correlation between the fluctuations of wind speed and air temperature will cause considerable variation in the sensible and the latent heat fluxes due to the products, $V_A(T_s - T_A)$ in Eq. 10 and $V_A[q_s(T) - q_A(T_C)]$ in Eq. 11 in Part I (YOON, 1982). Figure 3 shows the relation between the wind speed and air temperature at Vladivostok and Kimchaek (North Korea) in winter in 1967 (FUKUOKA and MISUMI, 1977). The fluctuation of wind speed has a period of several days and has a strong

negative correlation with air temperature. In order to include the effect of the negative correlation between the fluctuations of wind speed and air temperature, the following approximate formulae for V_A and T_A are used in Experiments II and III:

$$V_A = V_{A0}(x, y, t)[1 + \alpha(t) \sin(2\pi t/T_F)] \quad (13)$$

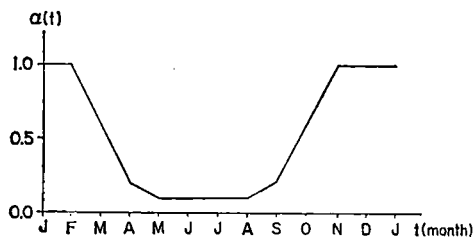


Fig. 4. Seasonal variation of the intensity of the short term fluctuation $\alpha(t)$.

and

$$T_A = T_{A0}(x, y, t) - 5.0\alpha(t) \sin(2\pi t/T_F) \quad (14)$$

where $V_{A0}(x, y, t)$ and $T_{A0}(x, y, t)$ are the above mentioned, linearly interpolated values of monthly mean wind speed and air temperature used in Experiment I, respectively. $\alpha(t)$ is the seasonal variation in the intensity of the short period fluctuations. The intensity is large in winter and $\alpha(t)$ is assumed as shown in Fig. 4. In this study, 6 days are taken as T_F .

5. Results

Initially, the ocean is filled with homogeneous water whose temperature is 1°C and salinity is 34.06‰ , which corresponds to the Proper Water in the Japan Sea.

In Experiment I, the lowest surface temper-

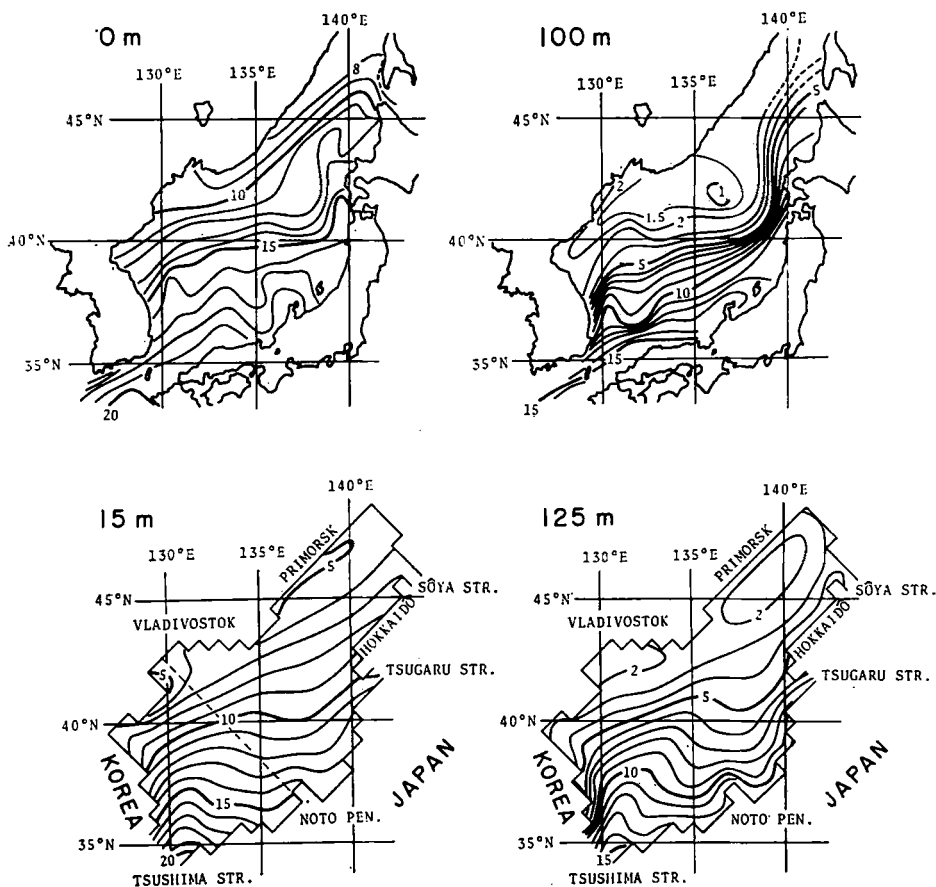


Fig. 5. Horizontal distributions of the annual mean observed temperature fields ($^\circ\text{C}$) at the sea surface and a depth of 100 m (upper: after Japan Oceanographic Data Center, 1975) and the calculated temperature fields at depths of 15 m and 125 m (lower).

ature in the model ocean in winter increases from year to year and becomes warmer than 2°C after time integration for four years. No formation of the Proper Water in the Japan Sea takes place in winter in this model. The time integration of Experiment II is carried out for seven years. The lowest surface temperature in winter in Experiment II does not become lower than 1°C and the formation of the Proper Water in the Japan Sea does not take place in Experiment II either, and so the results of Experiments I and II will not be discussed further. Other results of Experiments I and II are not very different from those of Experiment III.

5-1. Annual mean

The time integration in Experiment III is carried out for 9 years, to get a quasi-stationary state in the upper layer ($>400\text{ m}$) of the model ocean. Figure 5 shows the horizontal distributions of the annual mean temperature fields at depths of 15 m and 125 m in Experiment III. The corresponding observed temperatures at the ocean surface and at a depth of 100 m are also shown in Fig. 5 after JAPAN OCEANOGRAPHICAL DATA CENTER (JODC: 1975). Figure 6 shows the annual mean of the calculated velocity field at a depth of 15 m. The annual means of the oceanographical elements in Experiment III are obtained by taking the average for the last 365 days of the calculation period. Though the calculated temperature field at a depth of 15 m is a few degrees colder than that observed at the surface except in the region near the

Tsushima Strait, the synoptic patterns at the surface and 15 m are similar.

The isotherms of the observed temperature field at a depth of 100 m indicate the existence of two currents which branch near the Tsushima Strait. One of them which is called the East Korean Warm Current, flows northward along the Korean coast. The other flows along the Japanese coast and is called the nearshore branch current of the Tsushima Current. The calculated temperature field at a depth of 125 m indicates the existence of a strong current corresponding to the East Korean Warm Current and a weak boundary current along the Japanese coast. The calculated velocity field indicates a strong western boundary current along the Korean coast which corresponds to the large east-west temperature gradient. The maximum speed of the boundary current is 20.9 cm s^{-1} . The main part of the current flows north-eastward after separating from the Korean coast and diverges in the central region of the model ocean.

A weak boundary current, which is not so strong as the western boundary current along the Korean coast, flows along the Japanese coast. It is shown in Section 5-2 that this boundary current along the Japanese coast is conspicuous in summer and autumn. It should

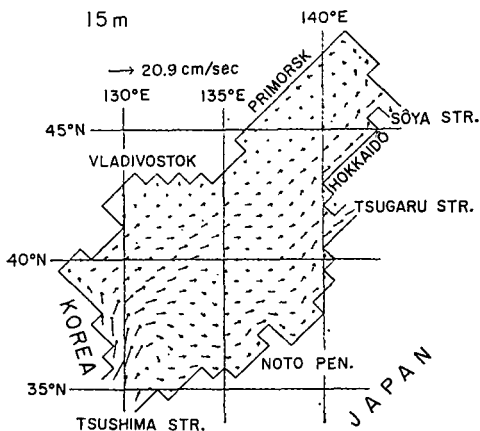


Fig. 6. Annual mean of the calculated velocity field at a depth of 15 m.

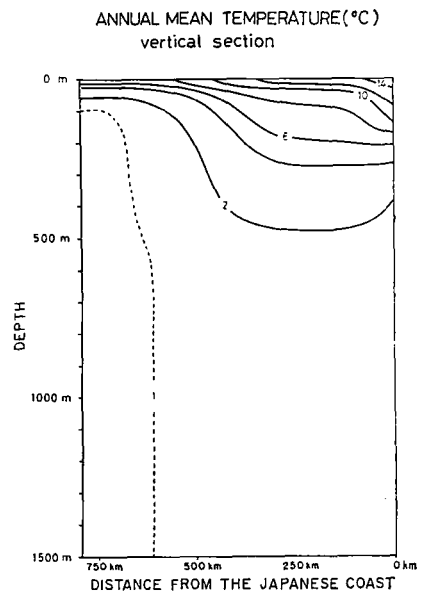


Fig. 7. Vertical section of the temperature field ($^{\circ}\text{C}$) along the dashed line shown in Fig. 5.

be noted that the clear splitting into two branches near the Tsushima Strait as seen in the observed temperature field in Fig. 5 is not obtained in this Experiment III.

Figure 7 shows the vertical section of the temperature field along the dashed line shown in Fig. 5. The dashed line shown in Fig. 7 indicates the isotherm of 1°C which is the temperature of the initially pre-existing water. The existence of the water with a temperature below 1°C indicates that formation of deep water takes place. Since the formation of subarctic water also takes place in the surface layer in the northern part of the model ocean in winter, a pronounced thermal front forms at a distance of about 450 km from the Japanese coast. This corresponds to the Polar Front in the Japan Sea, which is a boundary surface between the Subarctic Water and the Tsushima Warm Water. It roughly corresponds to the 6°C

isotherm at a depth of 100 m in Fig. 7. Another shallow front exists near the Japanese coast which indicates the existence of a boundary current along the Japanese coast.

Figure 8 shows the horizontal distributions of the annual means of the calculated salinity field at a depth of 125 m and the observed salinity field at a depth of 100 m. There are many discrepancies between the calculated and observed salinity fields, though the gross features of the calculated temperature fields (Fig. 5) are similar to those observed. High salinity water (>34.1‰) occupies the region along the Japanese coast in the observed salinity field at a depth of 100 m (Fig. 8: upper), while in the model low salinity water (<34.1‰) occurs in this region. In the model high salinity water (>34.1‰) occupies a tongue-like region (the shaded area in Fig. 8: lower) corresponding to regions of the strong western boundary current and its extension (see Fig. 6).

5-2. Seasonal variations

Figures 9 and 10 show the seasonal variations of the calculated temperature field at a depth of 125 m and the horizontal velocity field at a depth of 15 m, respectively, in the last year of the time integration. From January to March the formation of deep water takes place in the region along the Siberian coast. The synoptic pattern of the isotherms does not vary much during the period from January to June, though the isotherms have a tendency to shift southward from January to March as a result of cooling at the sea surface. From January to June, a large horizontal temperature gradient exists along the Korean coast which corresponds to the East Korean Warm Current. During the period from July to December, another pronounced horizontal temperature gradient appears along the Japanese coast, which corresponds to a narrow boundary current along the Japanese coast in Fig. 10. A density-driven boundary current also develops along the Primorsk in summer and autumn. This originates from the Tsushima Current.

Figure 11 shows the corresponding monthly variations of the calculated salinity fields at a depth of 80 m. The high salinity water (the shaded area >34.1‰), which flows into the model ocean through the Tsushima Strait in winter and spring, travels northward along the Korean coast due to advection by the western

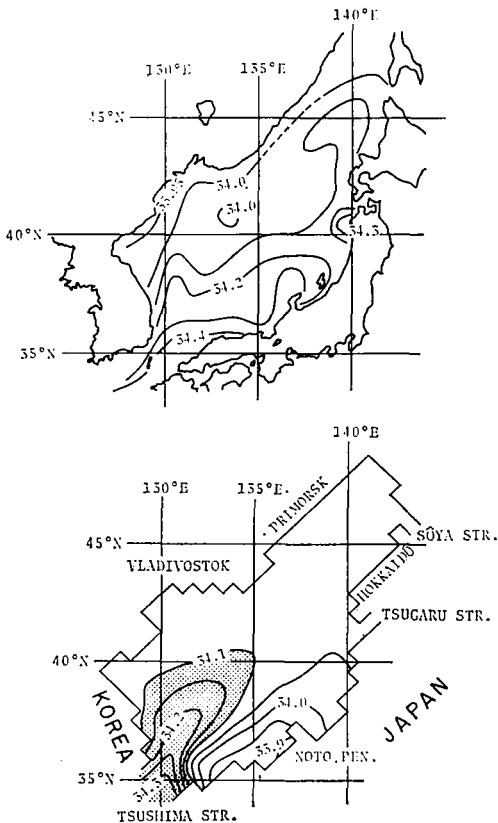


Fig. 8. Horizontal distributions of the annual mean observed salinity fields (‰) at a depth of 100 m (upper) and the calculated salinity fields at a depth of 125 m (lower).

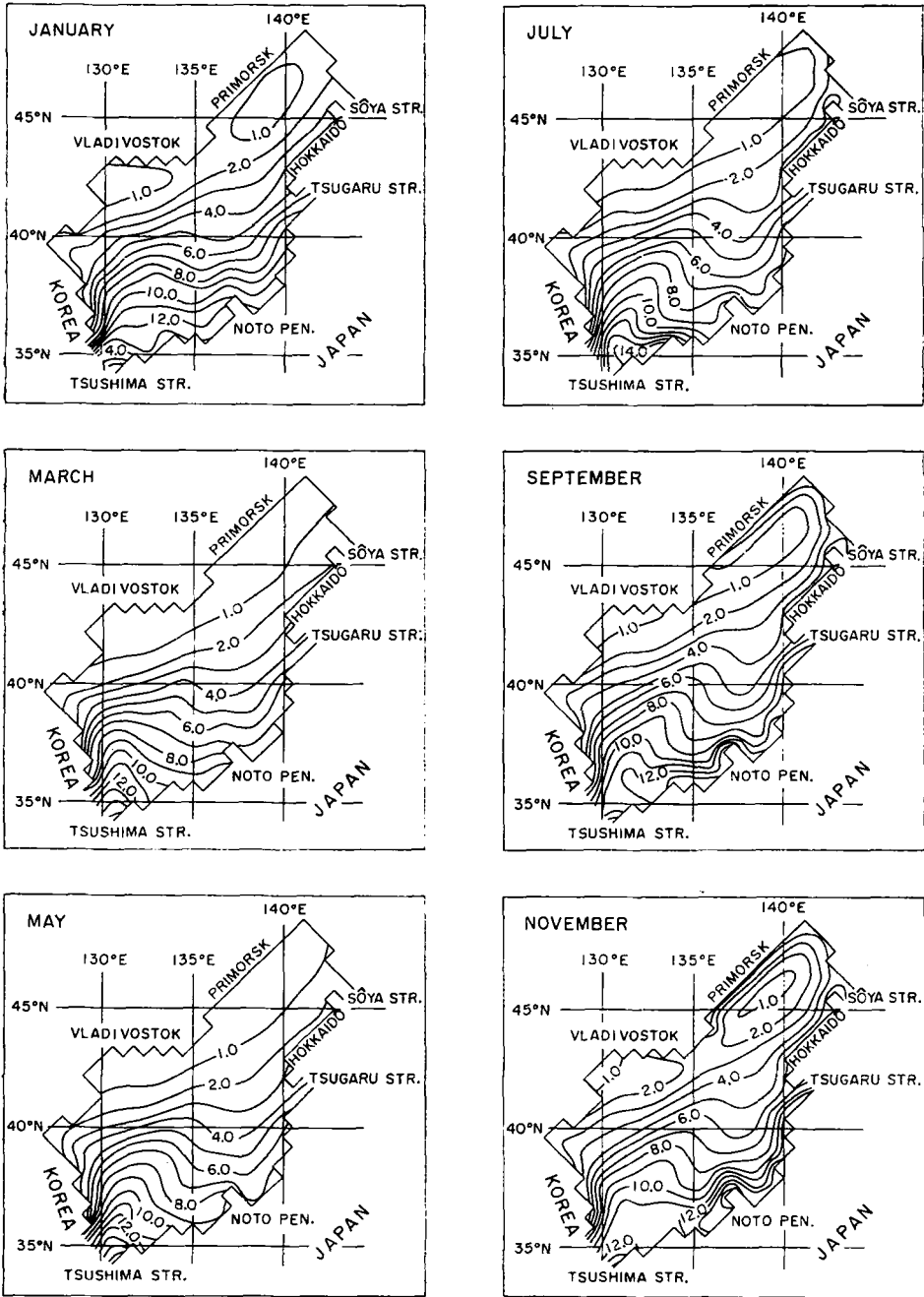


Fig. 9. Monthly variations of the calculated temperature field (°C) at a depth of 125 m in the last year of the time integration.

boundary current (the East Korean Warm Current) and continues to travel north-eastward forming a tongue-like saline region in the central portion of the ocean. It reaches the Tsugaru Strait within a year. The low salinity water (<34.1‰), which flows into the ocean through

the Tsushima Strait in summer and autumn, splits into two branches as is clearly shown in the distribution in September. One of the two branches of low salinity water travels along the Korean coast due to advection by the western boundary current (the East Korean Warm Cur-

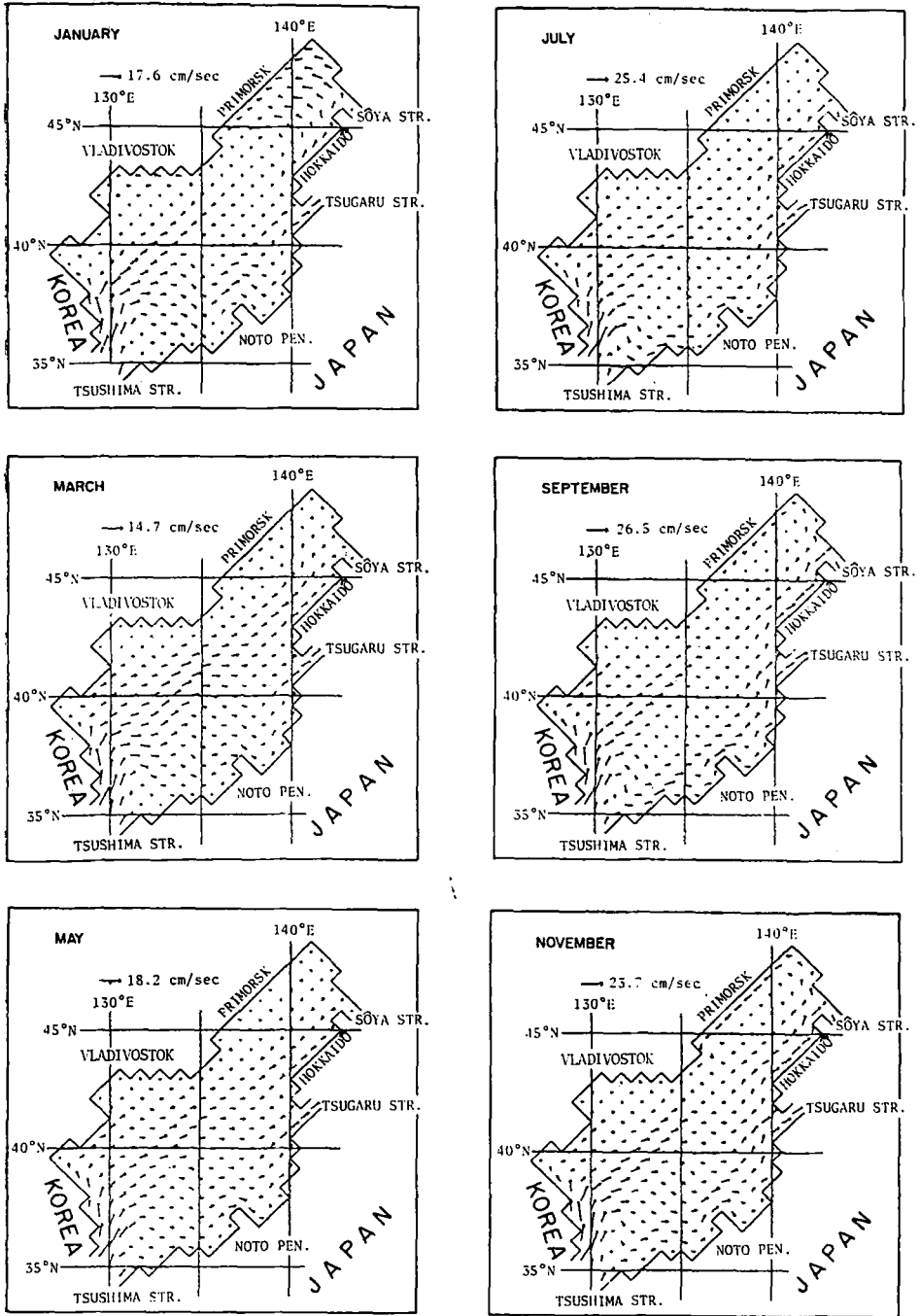


Fig. 10. Monthly variations of the calculated horizontal velocity field at a depth of 15 m in the last year of the time integration.

rent), and the other travels along the Japanese coast.

The width of the current which appears along the Japanese coast in summer and autumn is very narrow and comparable with the grid

interval in this calculation, which is taken to be a little larger than the Rossby's internal radius of deformation. In summer and autumn, the density difference between the interior water and the inflowing water becomes large as a

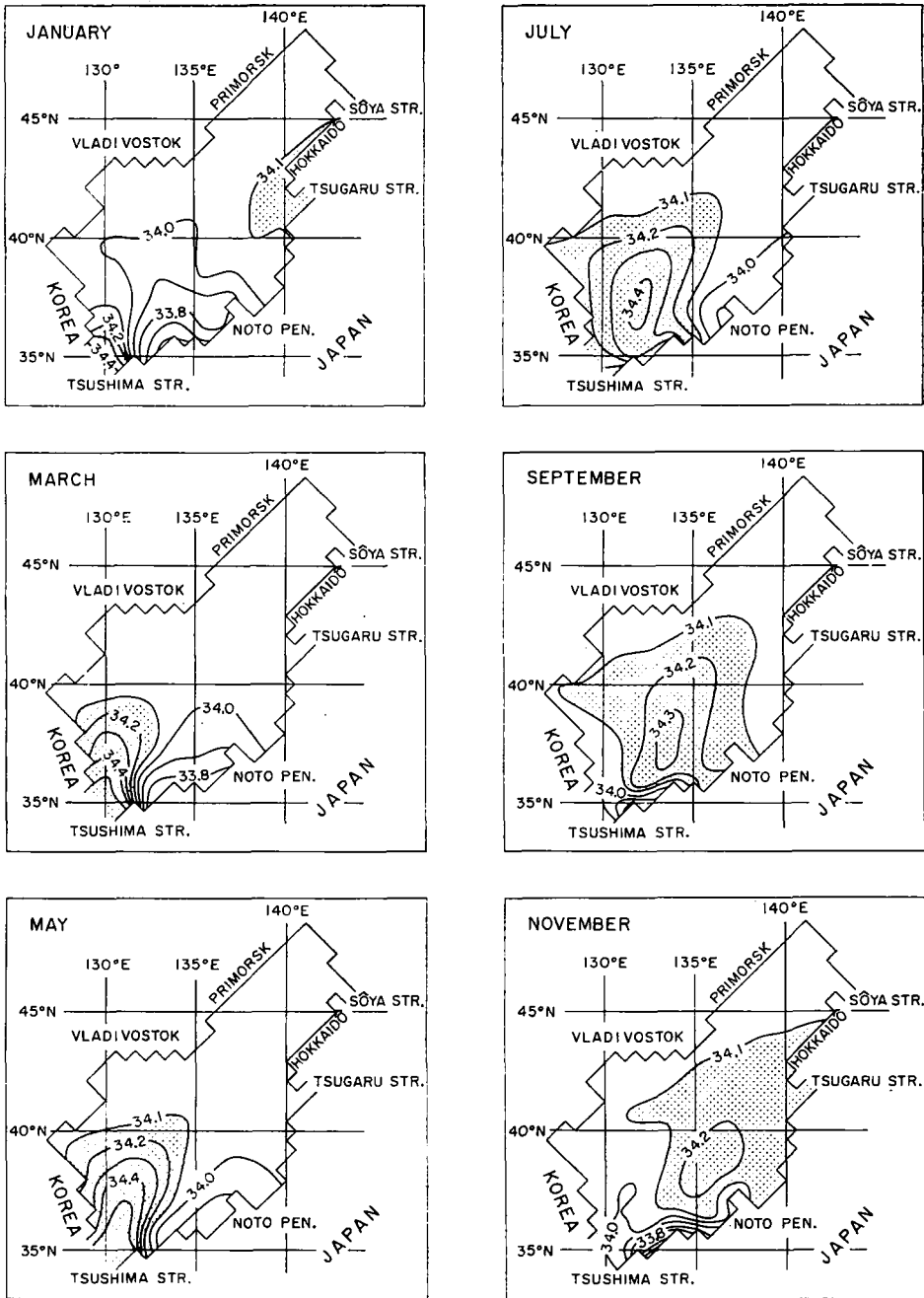


Fig. 11. Monthly variations of the calculated salinity field (‰) at a depth of 80 m in the last year of the time integration.

result of severe cooling of the interior water in winter and the warming and lowering of the salinity of the inflowing water in summer and autumn. From the narrowness and the direction of the current along the Japanese coast and the density difference between the interior and in-

flowing waters, this branch may be understood as a density-driven boundary current (YOON and SUGINOHARA, 1977).

By comparing the behaviour of the calculated salinity field with the monthly variations of the observed salinity field at a depth of 50 m reported

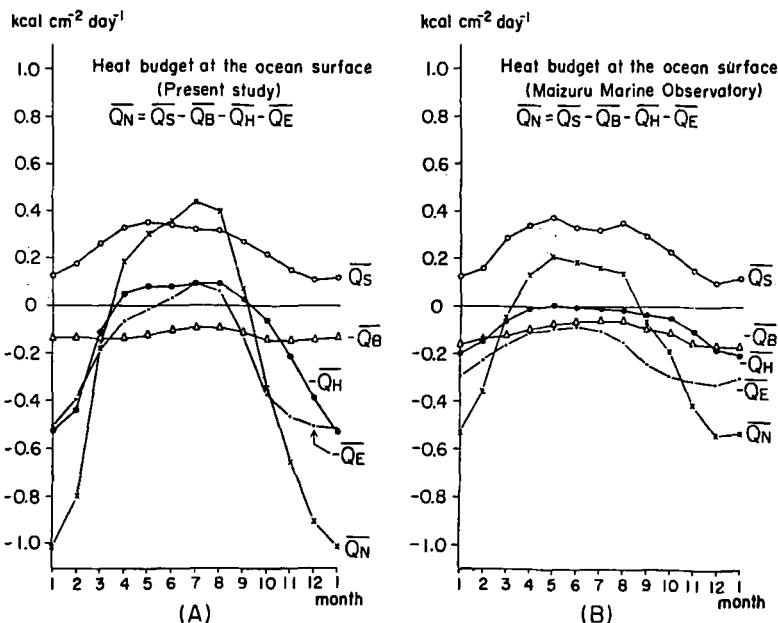


Fig. 12. Monthly variations of the components of the heat flux across the ocean surface; (A) is calculated in Experiment III and (B) was reported by Maizuru Marine Observatory.

by JODC (1978), great discrepancies can be seen between the calculated and observed salinity fields. The behavior of the high salinity water in particular differs greatly. The main part of the high salinity water which flows into the Japan Sea in winter and spring in the real ocean travels along the Japanese coast, while that in the model ocean travels along the Korean coast and the Polar Front.

As clearly seen from the calculated horizontal distribution of the salinity, the characteristics of the boundary current along the Japanese coast in the model, which appears from July to December, differs greatly from that of the near-shore branch of the Tsushima Current. So, it is concluded that Experiment III did not reproduce the real nearshore branch of the Tsushima Current.

5-3. Heat budget

Now, let us consider the heat budget in the model ocean by using the results of Experiment III. The total heat flux into the model ocean is given by the sum of the net downward heat flux across the ocean surface and the heat flux by advection through the three straits. If the total heat flux into the model ocean is denoted by Q , we have

$$Q = \iint_{\Gamma} Q_N d\Gamma + Q_{v1} + Q_{v2} + Q_{v3} \quad (15)$$

where Q_N is the net downward heat flux per unit area of the sea surface and Γ is the model ocean surface. The heat fluxes through the Tsushima Strait (Q_{v1}), Tsugaru Strait (Q_{v2}) and Sôya Strait (Q_{v3}) are defined by

$$Q_{vi} = C_{pw} \rho_0 \int_{A_i} T_i v_i dA \quad (16)$$

where C_{pw} ($=0.934 \text{ cal g}^{-1}$) is the specific heat of the sea water at constant pressure, ρ_0 (1.0 g cm^{-3}) the mean density of the sea water of the whole ocean, T the temperatures in the straits, A the transverse cross-sectional area of the straits, and v the velocity* normal to the transversal section of the straits respectively. The subscripts i (1, 2, 3) refer to the Tsushima-, Tsugaru- and Sôya Straits, respectively.

If we divide (15) by the sea surface area Γ , we have

$$\bar{Q} = \bar{Q}_N + \bar{Q}_{v1} + \bar{Q}_{v2} + \bar{Q}_{v3} \quad (17)$$

where an overbar indicates the areal average

* Inflow direction is taken to be positive.

of the property.

First, we estimate the value of \overline{Q}_N . It is divided into each component as

$$\overline{Q}_N = \overline{Q}_S - \overline{Q}_B - \overline{Q}_H - \overline{Q}_E \quad (18)$$

where Q_N is the solar radion, Q_B the back radiation, Q_H the sensible heat flux, and Q_E the latent heat flux from the ocean surface, respectively. Figure 12 shows the monthly variations of the components of the heat flux \overline{Q}_N across the ocean surface; (A) is calculated from the results in the last year of the time integration of Experiment III and (B) was reported by MAIZURU MARINE OBSERVATORY (MMO) (1972). The solar radiation \overline{Q}_S and the back radiation \overline{Q}_B in (A) are almost the same as their respective values in (B). The latent heat flux \overline{Q}_E and the sensible heat flux \overline{Q}_H in (A), which are upward in winter, have maxima in January. The maxima are almost twice those in (B). The directions of the latent heat flux and the sensible heat flux in (A) are downward from June to August and from April to September, respectively. In contrast, the directions of the latent heat flux in (B) are always upward and those of the sensible heat flux in (B) are upward except in May.

Next, each term of Eq. (17) is investigated except \overline{Q}_N . Figure 13 shows the monthly variations of the heat flux through the three straits. \overline{Q}_{v1} , $-\overline{Q}_{v2}$ and $-\overline{Q}_{v3}$ have their maxima in September or October and minima in March or April.

The annually averaged components of heat flux into the model ocean are shown in Table 4, where an asterisk indicates the annual mean of each component. Since the annual means of

net heat flux per unit area \overline{Q}_N^* across the model ocean surface and the total heat flux $\overline{Q}_{v1}^* + \overline{Q}_{v2}^* + \overline{Q}_{v3}^*$ through the three straits into the model ocean are $-181.5 \text{ cal cm}^{-2} \text{ d}^{-1}$ and $176.8 \text{ cal cm}^{-2} \text{ d}^{-1}$, respectively, the total heat flux \overline{Q}^* into the model ocean is calculated to be $-4.7 \text{ cal cm}^{-2} \text{ d}^{-1}$. This value of \overline{Q}^* indicates that the cooling of the ocean is still taking place at a rate on the order of one degree per 100 years if the entire water column from the bottom to the surface is cooled. This value is very small and as a result the temperature fields become almost steady at the end of the time integration. The time scale for attaining the steady state in Part I (YOON, 1982) is determined by the diffusion time ($H^2/K_v \sim 3,000$ years, where H is the depth of the ocean). In this model, the formation of the deep water takes place and cold water is

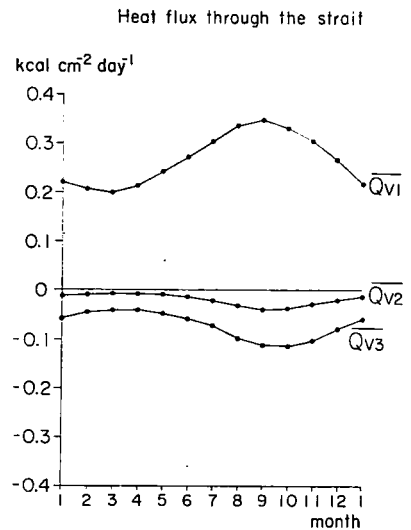


Fig. 13. Monthly variations of the heat fluxes through the three straits.

Table 4. Annually averaged components of heat flux. An asterisk (*) indicates the annual mean of each component. For indices see text.

Heat flux across the ocean surface ($\text{cal cm}^{-2} \text{ d}^{-1}$)			Heat flux ($\text{cal cm}^{-2} \text{ d}^{-1}$)	
Components	\overline{Q}_S^* (solar radiation)	249.7	\overline{Q}_{v1}^* (Tsushima Straits)	269.7
	\overline{Q}_B^* (back radiation)	123.3	\overline{Q}_{v2}^* (Tsugaru Straits)	-72.4
	\overline{Q}_H^* (sensible heat)	108.0	\overline{Q}_{v3}^* (Sôya Straits)	-20.5
	\overline{Q}_E^* (latent heat)	199.9		
Total	$\overline{Q}_N^* =$ $\overline{Q}_S^* - \overline{Q}_B^* - \overline{Q}_H^* - \overline{Q}_E^*$	-181.5	$\overline{Q}_v^* =$ $\overline{Q}_{v1}^* + \overline{Q}_{v2}^* + \overline{Q}_{v3}^*$	176.8

advected horizontally in a deep layer and balances the downward heat flux in warm water regions. The time scale of formation of the deep water is determined by $\frac{C_q}{C_{pv}H}$, where C_q ($\text{cal cm}^{-2}\text{d}^{-1}\text{deg}^{-1}$) is the heat flux coefficient at the ocean surface, and has a value of 2,000 days when $C_q \approx 100 \text{ cal cm}^{-2}\text{d}^{-1}\text{deg}^{-1}$. The advection time scale in the deep layer is L/v (L is the horizontal scale of the ocean and v is the horizontal advection velocity in the deep layer). This has a value of $10^3 \sim 10^4$ days with 1,000 km for L and $1 \sim 10 \text{ mm s}^{-1}$ for v . These time scales are in a good agreement with the integration time of the present experiment.

According to MIYAZAKI (1952), the heat flux through the Tsushima Strait corresponding to $\overline{Q_{v1}}^*$ is $289.8 \text{ cal cm}^{-2}\text{d}^{-1}$ and the sum of the heat fluxes through the Tsugaru- and the Sōya Straits is $206.0 \text{ cal cm}^{-2}\text{d}^{-1}$. The latter value is almost twice as much as the sum of $-\overline{Q_{v2}}^*$ and $-\overline{Q_{v3}}^*$ in the present study. It seems that we underestimate the heat flux $-\overline{Q_{v2}}^*$ and $-\overline{Q_{v3}}^*$ are underestimated in this study because the temperatures at the outflow openings are a few degrees lower than those observed, as shown in Fig. 5. If the temperatures at the outflow openings are a few degrees warmer, the heat flux through the two outflow openings will increase by about 50% of it in the present study. If we can reproduce a confined boundary current along the Japanese coast, the difference in temperature between the Tsushima- and the Tsugaru Straits may diminish and the heat flux across the ocean surface will be close to the value calculated from observed data.

6. Summary and conclusions

In winter and spring, the water supplied into the model ocean through the inflow opening flows northward along the Korean coast as a western boundary current corresponding to the East Korean Warm Current in the Japan Sea. In summer and autumn, the warm water splits into two branches (although this is not clear near the Tsushima Strait): one flows northward along the Korean coast from winter to spring and the other flows along the Japanese coast as a density-driven boundary current due to the inflow of the warm and low salinity water in

summer and autumn, which shows a large density contrast with the interior water which has been cooled during winter. The lack of a boundary current along the Japanese coast from winter to spring results in a large discrepancy between the calculated and observed salinity field distributions.

Seasonal variations of atmospheric conditions are essential to the formation of the deep water corresponding to the Proper Water in the Japan Sea.

Analysis of the heat budget, indicates that the flux through the outflow openings seems to be underestimated because the temperatures at the outflow openings are a few degrees lower than those observed. If a confined boundary current along the Japanese coast can be reproduced in the model, the difference in temperature between the Tsushima- and Tsugaru Straits may diminish and the heat fluxes across the ocean surface will have values close to those calculated from the observed data.

In this study, we neglected the effect of bottom topography. The offshore scale of the continental shelf and slope is on the order of 100 km. This corresponds to the scale of each branch of the Tsushima Current System. There is a strong possibility that the water flowing out of the Tsushima Strait is significantly controlled by the continental shelf and slope. That is, the flow will tend to follow the isopleths of bottom topography and will exist at all seasons as long as water is supplied to the ocean. This bottom controlled current existing at all seasons could advect the high salinity water along the Japanese coast. In the next paper of the present study (Part III: YOON, MS), the effect of bottom topography on the Tsushima Current will be examined.

Acknowledgements

The author expresses his hearty thanks to the late Professor Kozo YOSHIDA for his guidance and encouragement during this work.

References

- BRYAN, K. (1969): A numerical method for the study of the circulation of the world ocean. *J. Comp. Phys.*, **4**, 347-376.
 BUDYKO, M. L. (1974): *Climate and Life*. Academic Press, New York, 508 pp.

- DEACON, E. L. and E. K. WEBB (1962): Interchange of properties between sea and air. The Sea: Vol. 1, ed. by H. U. SVERDRUP, M. W. JOHNSON and R. H. FLEMING, Wiley Interscience, New York, pp. 49-87.
- FRIEDRICH, H. and S. LEVITUS (1972): An approximate equation of state for sea water, suitable for numerical ocean models. *J. Phys. Oceanogr.*, **2**, 514-517.
- FUKUOKA, J. and A. MISUMI (1977): Sinking in the Japan Sea. *Bull. Fac. Fish., Hokkaido Univ.*, **28**, 143-153.
- HANEY, R. L. (1971): Surface thermal boundary condition for ocean circulation model. *J. Phys. Oceanogr.*, **1**, 241-248.
- JAPAN METEOROLOGICAL AGENCY (1971): Climate Atlas of Japan. Vol. 1. Chijin-shokan, Tokyo, 59 pls.
- JAPAN OCEANOGRAPHIC DATA CENTER (1975): Marine Environmental Atlas: northwestern Pacific Ocean [I] (all months). Japan Hydrogr. Association, Tokyo, 157 plates.
- JAPAN OCEANOGRAPHIC DATA CENTER (1978): Marine Environmental Atlas: northwestern Pacific Ocean [I] (seasonal and monthly). Japan Hydrogr. Association, Tokyo, 164 plates.
- MAIZURU MARINE OBSERVATORY (1972): Marine meteorological study of the Japan Sea. *Tech. Rep. Japan Meteorol. Agency*, (80), 1-116.
- MIITA, T. (1976): Current characteristics measured with current meters at fixed stations. *Bull. Japan Soc. Fish. Oceanogr.*, **28**, 33-58.
- MIYAZAKI, M. (1952): The heat budget in the Japan Sea. *Rep. Hokkaido Reg. Fisher. Res. Lab.*, **4**, 1-45. (in Japanese).
- MUNK, W. H. (1950): On the wind-driven ocean circulation. *J. Meteor.*, **7**, 79-93.
- NAN'NITI, T. and A. FUJIKI (1967): Secular variations of hydrographic conditions in the East Tsushima Strait. *J. Oceanogr. Soc. Japan*, **23**, 201-212. (in Japanese).
- SHEPPARD, D. A. (1958): Transfer across the earth's surface and through the air above. *Q.J.R. Met. Soc.*, **84**, 205-224.
- YI, S. U. (1966): Seasonal and secular variations of the water volume transport across the Korea Strait. *J. Oceanogr. Soc. Korea*, **1**, 7-13.
- YOON, J. H. (1982): Numerical experiment on the circulation the Japan Sea. Part I: Formation of the East Korean Warm Current. *J. Oceanogr. Soc. Japan*, **38**, 43-51.
- YOON, J. H. (MS): Numerical experiment on the circulation in the Japan Sea. Part III: Formation of the nearshore branch of the Tsushima Current. *J. Oceanogr. Soc. Japan*, **38**(3) (in press).
- YOON, J. H. and N. SUGINOHARA (1977): Behavior of warm water flowing in to a cold ocean. *J. Oceanogr. Soc. Japan*, **33**, 272-282.

日本海の海洋循環についての数値実験

II. 対馬海流に対する気象条件の季節変動の影響

尹 宗 煥*

要旨: 対馬, 津軽, 宗谷海峡に相当する3つの海峡を持った水深一定の海のモデルを用いて, 対馬海流の季節変動についての数値実験を行なった。夏から晩秋にかけては, 東鮮暖流として北上する分枝流の他に, 冬季に冷却された日本海内部の水と, 対馬海峡から夏季に流入する高温, 低塩水との密度差が大きくなることによって日本沿岸に沿って北東に流れる(密度流としての)沿岸分枝

流が現われる。冬から初夏までの期間にはこの沿岸分枝流は消滅する。この結果, 日本沿岸沿いに高塩分水を運ぶことが不可能となり, 極前線沿いに高塩分水帯が出現することになる。これは実際の塩分分布とは大きな食い違いを見せており, 対馬海流の沿岸分枝が, 密度流としてだけでは説明されないことを意味している。また, 日本海固有水ならびに極前線の形成には, 気象条件の季節変化が重要であることも指摘される。

* 東京大学理学部地球物理学教室
〒113 文京区弥生2-11-16